JOURNAL OF GEOPHYSICAL RESEARCH, VOL. 114, A12216, doi:10.1029/2009JA014186, 2009

Shock aurora: Ground-based imager observations

X.-Y. Zhou,[1] K. Fukui,[2] H. C. Carlson,[3] J. I. Moen,[4] and R. J. Strangeway[5]

Received 20 February 2009; revised 28 June 2009; accepted 20 August 2009; published 23 December 2009.

[1] This paper studies dayside shock aurora forms and their variations observed by the ground-based all-sky imager (ASI) in Svalbard on 30 November 1997. The interplanetary shock arrived at Earth when Svalbard was at ~1120 magnetic local time. The ASI detected an auroral intensification by a factor of 2 or more in both green and red line emissions within 5 min after the shock arrival. The intensified green emissions were mainly diffuse aurora on closed field lines. They were latitudinally below and adjacent to the red aurora, which was mainly in the form of arcs and beams along the magnetic east-west direction. The diffuse aurora expanded equatorward and eastward, and its intensity exceeded the red arcs that were at ~5 kR. We confirmed that the eastward propagating diffuse aurora was actually moved antisunward along the oval, which suggests that the antisunward propagating shock aurora seen in space is mainly diffuse aurora. The intense diffuse aurora could be caused by wave instabilities led by a temperature anisotropy and/or caused by an enlarged loss cone. After the shock arrival, the detected low-latitude boundary of the cusp moved equatorward at a speed of ~18 km min^{-1}. As a result, the cusp meridional width was doubled from ~0.8° to 1.6° in latitude in 10 min. This finding implies that a low-latitude reconnection occurred during the compression. In this study the auroral signatures and speculated mechanisms are consistent with those revealed by in situ particle and wave observations from FAST and DMSP.

Citation: Zhou, X.-Y., K. Fukui, H. C. Carlson, J. I. Moen, and R. J. Strangeway (2009), Shock aurora: Ground-based imager observations, *J. Geophys. Res.*, *114*, A12216, doi:10.1029/2009JA014186.

1. Introduction

[2] As a geographic frontier in the sunward direction, the dayside auroral ionosphere first and directly reacts to the solar wind–magnetosphere–ionosphere interaction. Therefore, it is reasonable to expect that dayside auroral behavior is significantly different from that of nightside aurora. In general, dayside aurora is caused by soft electrons with average energy of ~100 eV at altitudes higher than nightside aurora. Red (OI, 630.0 nm) auroral intensity is about an order higher in intensity, and green (OI, 557.7 nm) auroral intensity is about an order lower than nightside auroras [*Sandholt et al.*, 2002].

[3] The latitudinal location of cusp auroral bands is strongly related to the interplanetary magnetic field (IMF) clock angle, θ [*Sandholt et al.*, 1998a; *Farrugia et al.*, 1998]. The auroral bands locate at ~78°–79° magnetic latitude (MLAT) for $\theta < 45°$, at high and low MLAT for θ within ~45°–90°, and only at low MLAT for $\theta > \sim 90°$. A poleward expansion of the cusp auroral bands might be an ionospheric signature of a flux transfer event [*Eather*, 1985; *Mende et al.*, 1998]. When the IMF B_z suddenly turns from large negative to large positive, red auroral locations switch origins from the cusp/low-latitude boundary layer to cusp/mantle, which *Sandholt et al.* [1996] interpreted as the switch of reconnection site from low-latitude to high-latitude magnetopause. In addition, dayside pulsating diffuse aurora at 557.7 nm is caused by dispersed field-aligned electrons accelerated near the equatorial plane [*Lorentzen et al.*, 1996; *Lorentzen and Moen*, 2000]. All these findings confirmed that dayside auroras can play key roles in understanding the solar wind–magnetosphere–ionosphere coupling. *Moen et al.* [1998] have pointed out that a red auroral arc is a unique footprint of dayside magnetic reconnection, which is the only known mechanism of bulk particle injection onto the dayside ionosphere.

[4] In addition to IMF direction effects, *Sandholt et al.* [1994] reported that the solar wind ram pressure evidently affects auroral motion in the cusp. With a strong and isolated pressure increase ($\Delta p/p \geq 0.5$), the green aurora shifted to lower latitudes. With a brief pressure pulse ($0.1 < \Delta p/p < 0.5$), the prenoon aurora moved eastward during negative IMF B_y and moved westward during positive B_y. However, with geographic constraints and sunlight contamination, the ground-based dayside auroral imaging has not been able to provide as much information as nightside observations concerning auroral small-scale structures (called auroral forms hereafter). Most of the time,

[1]Jet Propulsion Laboratory, Pasadena, California, USA.
[2]Air Force Research Laboratory, Hanscom AFB, Massachusetts, USA.
[3]Air Force Office of Science Research, Arlington, Virginia, USA.
[4]Department of Physics, University of Oslo, Oslo, Norway.
[5]Institute of Geophysics and Planetary Physics, UCLA, Los Angeles, California, USA.

0148-0227/09/2009JA014186$09.00

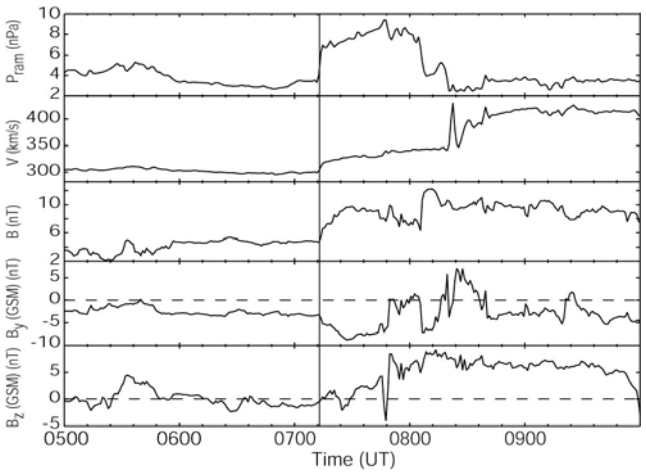

Figure 1. Solar wind and IMF data for the interplanetary shock obtained with the Wind spacecraft at ~0714 UT on 30 November 1997.

meridian-scanning photometer (MSP) data are the major data source for cusp and dayside auroral investigations.

[5] Space-based UV imaging has revealed that dayside aurora not only occurs along the oval but also expands to lower MLAT of ~65° during intense magnetospheric compression [*Liou et al.*, 2002; *Zhang et al.*, 2002; *Hubert et al.*, 2003; *Fuselier et al.*, 2004]. This discovery indicates that, in addition to magnetic reconnection, other mechanisms must exist for dayside auroral formation. Although various mechanisms have been proposed, such as adiabatic compression and field-aligned currents, none of them has been tested using identified auroral forms that are manifestations of specific particle acceleration mechanisms [*Zhou et al.*, 2008]. To obtain these auroral forms, the ground-based all-sky imager (ASI) needs to be in operation at (or near) local noon when a shock arrives, which rarely happens. This study examines dayside shock-caused auroral forms and their variations. Mechanisms of particle acceleration are identified and discussed accordingly.

2. Interplanetary Shock on 30 November 1997

[6] Figure 1 shows the interplanetary shock that was detected at ~0714 UT when the Wind spacecraft was at (196, 4, 27 R_e) (in GSM coordinates). At the shock, the solar wind ram pressure ($P_{\rm ram} = \rho V^2$) increased from ~3 to 6 nPa due mainly to an increase in proton density from ~20 to 35 cm^{-3}. The solar wind speed was low and had a minor enhancement at the shock from ~300 to 320 km s^{-1}. The IMF magnitude increased from ~5 to 7 nT at the shock and kept increasing to 10 nT by ~0730 UT. The IMF B_y component was negative in the shock upstream and turned further negative downstream of the shock, from −3 to −5 nT, and was −9 nT by ~0730 UT. The IMF B_z was near zero before and at the shock and turned to farther northward, then varying between ~2 and −2 nT prior to ~0730 UT. The calculated shock normal is (−0.92, 0.20, −0.34) in GSM coordinates (Y.-L. Wang, private communication, 2009). The shock Mach number is 1.2, with a shock speed of ~350 km s^{-1} along the normal direction. This shock caused a geomagnetic sudden commencement (SC) at ~0809 UT, determined from the NOAA National Geophysical Data Center database (http://www.ngdc.noaa.gov/stp/GEOMAG/geomag1.html). SC times have been widely used as a signature of interplanetary shock arrivals at the magnetopause [e.g., *McKenna-Lawlor et al.*, 2002]. The SC was accompanied by a significant dayside auroral response.

3. Ground-Based Auroral Observations

[7] The ASI in Ny Ålesund (75° MLAT) is an intensified silicon intensifier target TV camera system. It monitors auroral 2-D dynamic behavior in a large field of view (160° for 557.7 nm and 150° for 630.0 nm). The imaging observations are of the auroral green (557.7 nm) and red (630.0 nm) line emissions corresponding to transitions from ^{1}S and ^{1}D metastable states of oxygen (OI), respectively. It is assumed that the OI^{1}S emission layer is mainly near 150 km and caused by harder electrons and that the OI^{1}D emission layer is near 250 km and caused by softer electrons. At the SC time of 0809 UT on 30 November 1997, Ny Ålesund was at ~1120 magnetic local time (MLT). Figure 2 shows the auroral green line emissions for the shock aurora from 0808:15 to 0824:15 UT. The white arrow in the first image points toward magnetic north. The shock arrival is marked by a black arrow at the top. From 0808:15 to 0814:46 UT we used the highest image cadence, of ~30 s, to monitor how the green emissions changed during the most intense compression. Projected to ~150 km altitude, the green image covers a circular area with a radius of ~850 km. Before the shock arrival, there were some auroral beams (such as those marked by the white arrows in the second image) with "intensity" at ~630 counts. (Because the camera is not calibrated, the ASI "intensity" here and thereafter means an instrument response in counts per sample in the 2 s exposure time.) After 0809:15 UT, the magnetic southwest quadrant was illuminated first by diffuse aurora, which indicated a response time within ~30 s. The beams near the poleward boundary were not intensified evidently and had an intensity of ~630 counts (such as those marked by the white arrows in the third image). At 0809:45 UT, the diffuse auroral intensity increased to ~1000 counts. By 0810:15 UT the entire southern sky was covered by diffuse aurora. The auroral intensity reached its maximum at 0811–0813 UT at ~1600 counts. By 0824:15 UT, which was ~15 min after the shock arrival, the auroral intensity had recovered to the level prior to the shock arrival, although minor intensifications still maintained for some additional time.

[8] Figure 3 shows the auroral red line emissions in the same format as for Figure 2 but projected to ~250 km altitude. The image covers a sky circle area with a radius of ~930 km. In contrast to the green emissions, the red auroral emissions appeared as arcs and beams crossing the sky roughly in the magnetic east-west direction at higher latitudes but closely adjacent to the green line emissions. Prior to the shock arrival, the brightest aurora was $\lessapprox$1000 counts. At 0809:30 UT, right after the shock arrival, the auroral intensification occurred gradually, which is significantly different from the abrupt and intense response in green emissions. The noticeable auroral intensification started from 0811:00 UT,

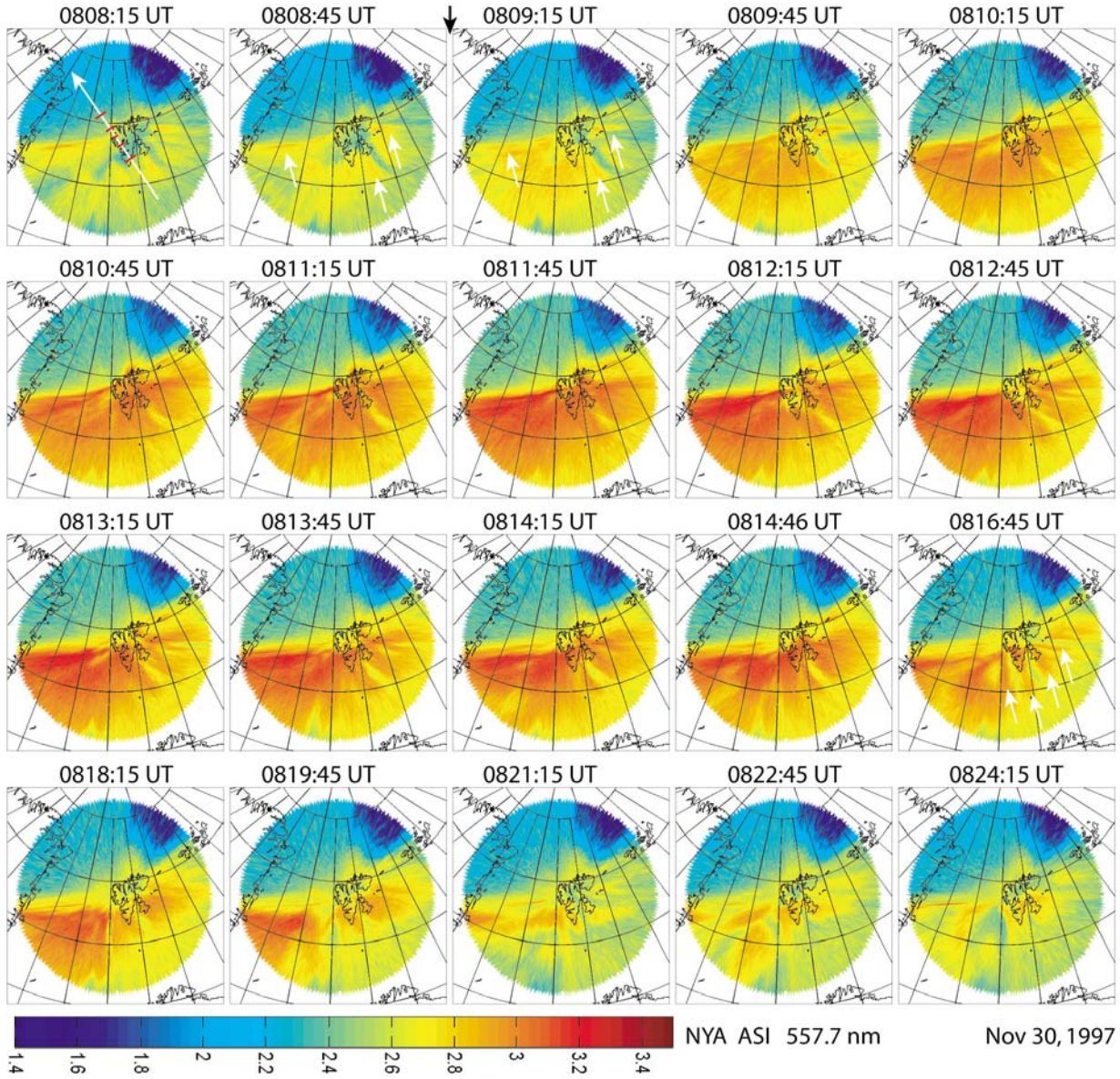

Figure 2. Ny Ålesund 557.7 nm green line emissions of the shock aurora on 30 November 1997. Grids in images are in geographic coordinates. The highest image cadence is used within the first 5 min after the shock arrival to show the auroral response. Afterward, a 1.5 min cadence is used to cover a longer time interval. In the first image, the white arrow points to the magnetic north and indicates the MSP scanning direction. Ticks on the arrow provide local zenith angles with the shortest at 0°, then 20° and 60° on each side to facilitate the comparison with MSP data in Figure 4. The black arrow on top shows that the shock arrival time at Earth was between 0808:45 and 0809:15 UT (SC at ∼0809 UT) when Svalbard was at ∼1120 MLT. The color bar on the bottom indicates the logarithm (base 10) of the sensor response rate, which is proportional to the auroral emission intensity.

when the arc projected into the eastern sky became brighter and reached ∼1300–1500 counts. The aurora was intensified gradually in the ASI images. From 0812:00 UT, the eastern arc intensity was saturated at ∼1600 counts. By 0824:31 UT, which is 15 min after the shock arrival, the red aurora did not start decaying as the green aurora did. Instead, the auroral intensity remained approximately unchanged until ∼0900 UT (data not shown but will be discussed in Figure 4). There was little intensification in red diffuse aurora in the southern sky. The intensity was ∼400–500 counts.

[9] Another optical instrument in Ny Ålesund is a multichannel MSP system that is sensitive to the green and red emissions. This calibrated MSP has a 2° angular resolution and scans roughly along the magnetic meridian (shown by the white arrows in Figures 2 and 3) from zenith 60°N to 60°S with a scan period of 18 s. Figure 4 presents green (Figure 4, left) and red (Figure 4, right) MSP scans of this shock aurora event. Figure 4 (left) shows that a sudden intensification of green aurora started from the southern limit of the MSP with a brightness jumping from 1 to 2 kR to a level greater than 5 kR, which caused the saturation.

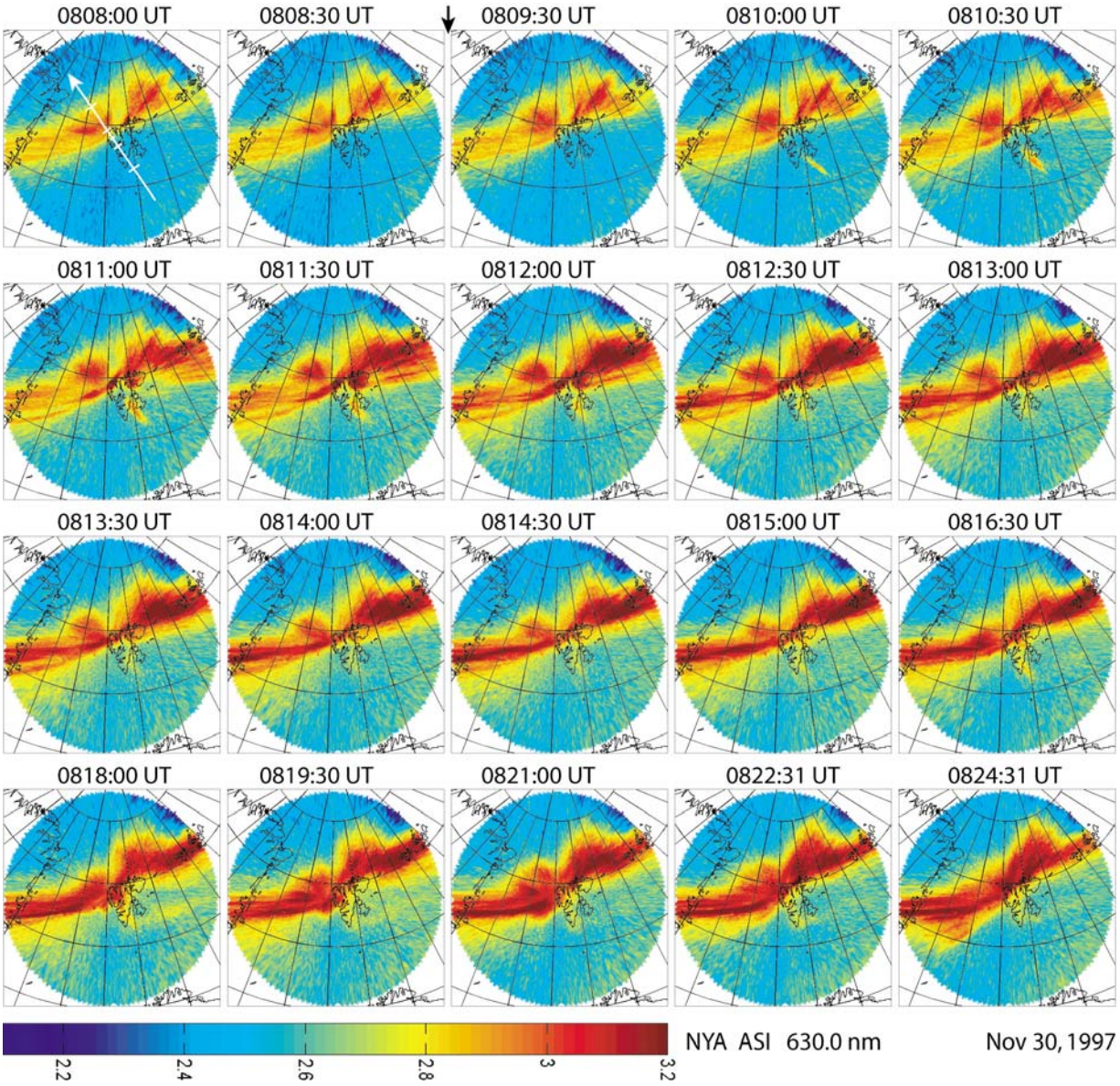

Figure 3. Ny Ålesund 630.0 nm red line emissions of the shock aurora on 30 November 1997. Figure format is the same as for Figure 2.

Then, the entire southern sky brightened from 0810 UT as an arc developed in the northern sky (~20°N) and rapidly moved southward to ~11°S which is consistent with Figure 2. The green line aurora in the cusp slightly increased in intensity from ~1.3 to 2 kR. Aurora along the southern magnetic meridian started declining from ~0817 UT.

[10] Figure 4 (right) shows that the red auroral intensification started mainly in the cusp from ~0809 UT at ~40°–60°N from ~4 to 5 kR, but such increases were not noticeable in ASI images. A particular point of interest is that the low-latitude boundary of the cusp moved southward from ~30°N to 10°S (scan angles) at ~0809–0819 UT, which was ~1120 MLT. The corresponding boundary motion speed is ~18 km min^{-1}. At the end of this interval, the latitudinal width had increased by a factor of ~2, from ~0.8° to 1.6° in latitude. Because of the MSP's narrow field of view and its meridian scan direction, most auroral intensifications as seen in the ASI images (shown in Figure 3) were not detected by the MSP. This finding again indicates the value of ASI data.

4. Discussion and Conclusion

4.1. Diffuse Dayside Aurora Caused by the Shock Impingement

[11] Both ASI images and MSP scans confirmed that the interplanetary shock caused a significant green auroral intensification by a factor of at least 2. The enhanced green aurora was mainly diffuse aurora in the southern sky with a prompt response within 30 s of shock arrival, on the basis of the highest image cadence of 30 s. For electrons of 1–10 keV, the bounce period between two hemispheres at ~75° MLAT is less than 10 s (X. Lin, private communication, 2007). That predicts a response time at ~5 s or less in the green diffuse aurora. In the first 2–3 min after the shock arrival, the lower-latitude diffuse green intensity exceeded

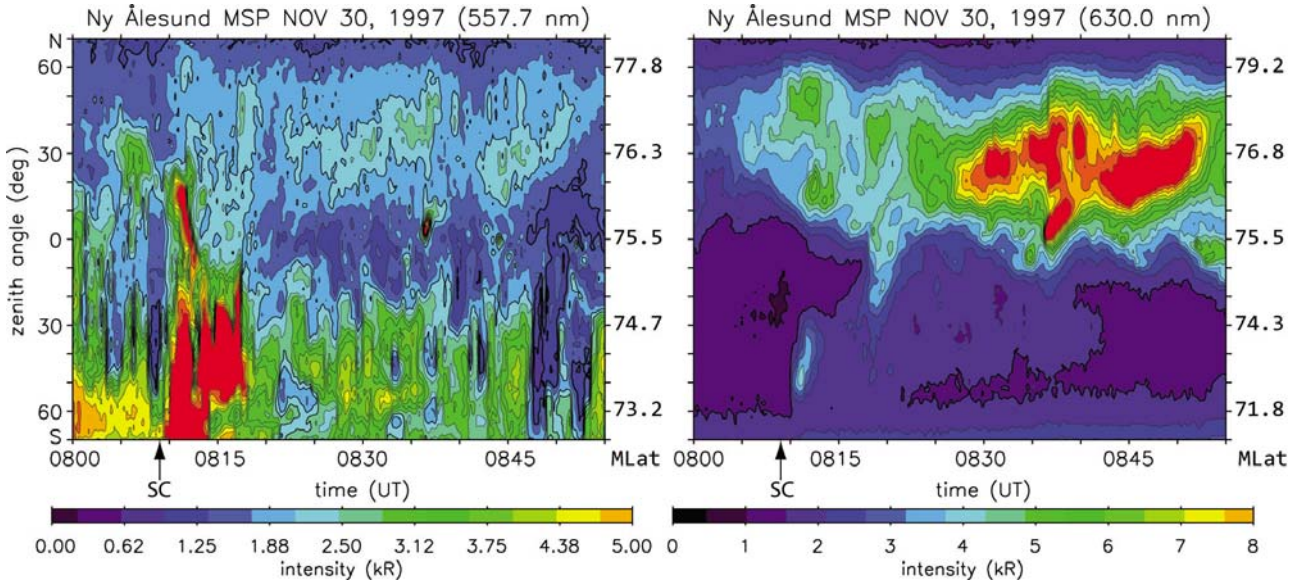

Figure 4. North-south MSP magnetic meridian scans of the (left) auroral green and (right) red emissions on 30 November 1997, taken with the narrow-field-of-view MSP. Two arrows on the bottom of MSP mark the SC time of 0809 UT; that is, the shock arrived at 0809 UT ± 15 s. Ticks on right of both images are corresponding magnetic latitudes in degrees. Ticks on left are zenith angle in degrees.

that of the poleward red aurora, the intensities of which were at ~5 kR (see Figure 4). This situation is rare, whether for dayside or nightside auroral activity.

[12] In the compressed dayside outer magnetosphere, the plasma density is relatively uniform in space compared with that of the region close to the ionosphere in high latitudes; the aurora caused by the scattered particles in the loss cone is, therefore, lacking in structures (i.e., the diffuse aurora). However, when the plasma density fluctuates, the diffuse auroral brightness varies, analogous to clouds in the sky. Such temporal and spatial variations are shown in Figure 4 (left) in the southern magnetic meridian.

[13] In general, diffuse aurora comprises auroral emissions that are relatively weak in intensity and lacking in structures (or sharp-edged structures). These characteristics imply a lack of structure in the source region where there are preexisting electrons and the "accelerators" that drive the electrons into the loss cone. This region can be very far from the ionosphere in the magnetosphere. For diffuse shock aurora, the accelerators are believed to be near the equator in the outer magnetosphere [*Zhou and Tsurutani*, 1999; *Tsurutani et al.*, 2001a, 2001b]. During a shock compression, plasma temperature anisotropies naturally develop. One explanation is that the first adiabatic invariant is conserved. Therefore, when B increases, an enhanced $T_\perp$ leads to $T_\perp/T_\parallel > 1$. This is the so-called adiabatic compression. Another explanation is that because $T_\parallel$ and $T_\perp$ satisfy the complex Ginzburg-Landau equations with $T_\perp \propto B$ and $T_\parallel \propto n^2/B^2$ [*Hellinger et al.*, 2003], the shock compression naturally leads to $T_\perp/T_\parallel \propto B^3/n^2 > 1$.

[14] The temperature anisotropy $T_\perp/T_\parallel > 1$ (i.e., departure from an isotropic Maxwellian particle distribution function) represents a possible source of free energy for different instabilities that grow in collisionless plasmas at frequencies below the electron cyclotron frequency [*Gary and Cairns*, 1999]. The instabilities include whistler, electrostatic, and z modes. The whistler mode requires the smallest anisotropy threshold, but the z mode requires a large temperature anisotropy. When the instability grows, wave-particle interactions lead to an enhancement of pitch angle scattering. Isotropic particles become profuse. As a result, diffuse aurora in the ionosphere occurs or becomes more intense. For example, the shock caused dayside proton aurora in the subaurora region. When the shock compression leads to proton temperature anisotropy, it provides the free energy source for the electromagnetic ion cyclotron wave instability. This instability has maximum growth rate at propagation parallel or antiparallel to the magnetospheric magnetic field, so that protons (and electrons) are predominantly pitch angle scattered by the wave [*Fuselier et al.*, 2004; *Yahnina et al.*, 2008].

[15] In addition to pitch angle scattering, the size of loss cone may be enlarged during the compression. The size is determined by

$$\theta = \sin^{-1}\sqrt{\frac{B_{\mathrm{eq}}}{B_i}}, \tag{1}$$

where θ is the half angle of the loss cone, B_{eq} is the geomagnetic field magnitude at the equator, and B_i is the geomagnetic field in the ionosphere. When B_{eq} increases because of the shock compression, B_i does not change. Therefore, the loss cone becomes larger. Consequently, more electrons precipitate into the ionosphere and cause diffuse aurora. For example, giving B_{eq} = 84 and 284 nT at the geosynchronous orbit before and after shock compression, respectively, and B_i = 48,900 nT at 66° latitude, θ increases from ~2.4° to 4.4°. The change of the electron flux in the loss cone is $F_2/F_1 = \tan\theta_2/\tan\theta_1 \approx 2$, where subscripts 1 and 2 indicate before and after the shock compression, respectively. Figure 2 shows that the diffuse auroral intensity increased by a factor of 2–3, which is consistent with this estimation.

[16] There are near-Earth satellite observations of other shock aurora events from FAST and DMSP. The in situ

observations from crosses of the oval in 0600–0900 MLT revealed that high-energy electrons (~1–10 keV) were highly isotropic and filled the loss cone [*Zhou et al.*, 2003]. The high-energy electrons appeared at lower magnetic latitudes adjacent to the poleward boundary. The electron energy flux increased about 1 order of magnitude after the shock arrival. These signatures are consistent with the preceding explanations in this section and the ground-based image observations shown in Figure 2 when the ASI was at ~1120 MLT. FAST data showed that the isotropic high-energy electrons can reach ~65° MLAT at ~0730 MLT, and DMSP data showed they can reach ~61° MLAT at ~0900 MLT. Other UV imaging observations showed that both electron and proton auroras occurred in ~60°–70° MLAT after shock compressions [*Liou et al.*, 2002; *Zhang et al.*, 2002; *Hubert et al.*, 2003; *Fuselier et al.*, 2004; *Meurant et al.*, 2004]. These findings are consistent with observations of the 30 November 1997 event. Some differences might exist between the processes at noon and in the dawn (or dusk) sector. With regard to the diffuse aurora on the closed file lines, the subauroral emission down to low latitudes ~60° MLAT near local noon may not occur at 0600 MLT and 1800 MLT because the compression effect reduces toward dawn and dusk flanks. With regard to the discrete aurora, in addition to the magnetic reconnection, kinetic Alfvén waves can also be generated by the magnetic shearing, which has been discussed by *Zhou et al.* [2003]. From our understanding of the shock aurora mechanisms, we can expect that in situ observations will not differ much between 1200 and 0900 MLT.

[17] With high time resolution images, the shock propagation effect can be identified. In Figure 2 from 0809:15 to 0810:45 UT, an auroral equatorward expansion occurred, indicated by gradually enhanced auroral intensities near the southern edge. This is because the outer magnetosphere was compressed sequentially from the magnetopause toward Earth while the shock propagated downstream. In addition to this latitudinal effect, the aurora expanded eastward (i.e., the southwest quadrant was illuminated first at 0809:15 UT and then the southeast quadrant at 0810:45 UT). We believe that this longitudinal expansion is the ionospheric effect of the shock tailward propagation that has been detected as an antisunward propagation along the oval by the space-based UV imagers [*Zhou and Tsurutani*, 1999; *Vorobjev et al.*, 2001; *Meurant et al.*, 2003, 2004]. Locally, the antisunward direction is eastward or westward depending on the relative location of the ground-based ASI and the shock touchdown local time. In this 30 November 1997 event, Svalbard was prenoon at ~1120 MLT, and the shock touchdown location was near 1110 MLT. So an antisunward propagation seen at Svalbard was first eastward toward local noon and Ostrov Zemlya Aleksandry, Russian Arctic islands.

[18] The mechanisms discussed here apply to the proton aurora as well. *Meurant et al.* [2003, 2004] have shown shock-triggered proton auroras that brightened near local noon and then propagated antisunward along the oval. The aurora was brighter in the duskside than that in the dawnside, which is consistent with the azimuthal drift of newly injected ions. Because proton precipitation enhances the ionospheric ionization, the secondary auroral electrons can excite transitions usually attributed to the electron aurora.

[19] Similar to the green aurora, weak diffuse red aurora also occurred at the ~2 kR response to the shock impingement. If the red aurora is caused by soft electrons of less than 1 keV (such as reported by *Shepherd et al.* [1980]), theoretically the expected response time is longer than that of the green diffuse aurora. This is because soft electrons of 0.1–1.0 keV have bounce periods in 20–60 s of the mirror motion in a dipole magnetic field [*Parks*, 2003]. In Figure 4, the red diffuse aurora in the southern sky had a short delay of ~30 s compared with the green diffuse aurora, which is consistent with this scenario.

4.2. Discrete Dayside Aurora Caused by the Shock Impingement

[20] Different from the green aurora, the enhanced red arcs shown in Figure 3 were either at the poleward boundary of the cusp or in the cusp. The red arcs were gradually intensified by a factor of ~2 in ~90–120 s after the shock arrival. The slow response might be due to a sensitivity threshold effect and the collisional quenching during the electron precipitation. The red auroral arcs also appeared to be relatively stable in the 30 s time scale (i.e., there were no abrupt morphology and intensity variations). This stability might be because the red arcs are confined to the ionospheric footprints of the magnetopause, which form the cusp boundary along the east-west direction. This spatial signature is different from nightside red arcs that are always dancing, bouncing, wiggling, and moving around in the entire field of view of an ASI, such as those during substorm expansion phases.

[21] The confinement makes the red arc a good indicator of dayside reconnection, which has been reported by *Sandholt et al.* [1994, 1998b, 1998c]. *Zhou et al.* [2003] have shown that low-energy electron (<1 keV) precipitation suddenly increased along the auroral poleward boundary right after the shock impingement. These electrons are accelerated field aligned and along highly structured field-aligned currents. Figure 5 shows the electron energy spectrum (Figure 5, left) and phase distribution (Figure 5, right) observed by the FAST satellite during a shock aurora event on 4 August 1997. This is the second event discussed by *Zhou et al.* [2003]. The phase distribution shows that the soft electrons (<1 keV as shown in Figure 5, left) were accelerated bidirectionally along the magnetic field. Such electrons are typically accelerated by kinetic Alfvén waves [*Wygant et al.*, 2002] at high altitudes, where the wave phase speed becomes comparable to electron thermal speeds, or inertial Alfvén waves [*Chaston et al.*, 2008] at altitudes where the perpendicular wavelength becomes comparable to the electron skin depth. *Wygant et al.* [2002] noted that on the nightside the transition from kinetic to inertial Alfvén waves occurred at altitudes of about 5 Earth radii. This transition is likely to occur at a somewhat different altitude on the dayside. *Wygant et al.* [2002] also noted that other authors [e.g., *Lysak and Lotko*, 1996] used the phrase "kinetic Alfvén waves" for waves that departed from the ideal MHD limit, regardless of whether the nonideal nature of the waves was from the effects of electron pressure (kinetic) or electron inertia. We will adopt the same approach here; the main effect is that the "kinetic" Alfvén waves have a parallel electric field associated with them that can accelerate electrons. This ability to accelerate electrons indicates that the highly structured field-aligned currents are very well related to kinetic Alfvén waves that can be generated by magnetic reconnection [*Stasiewicz et*

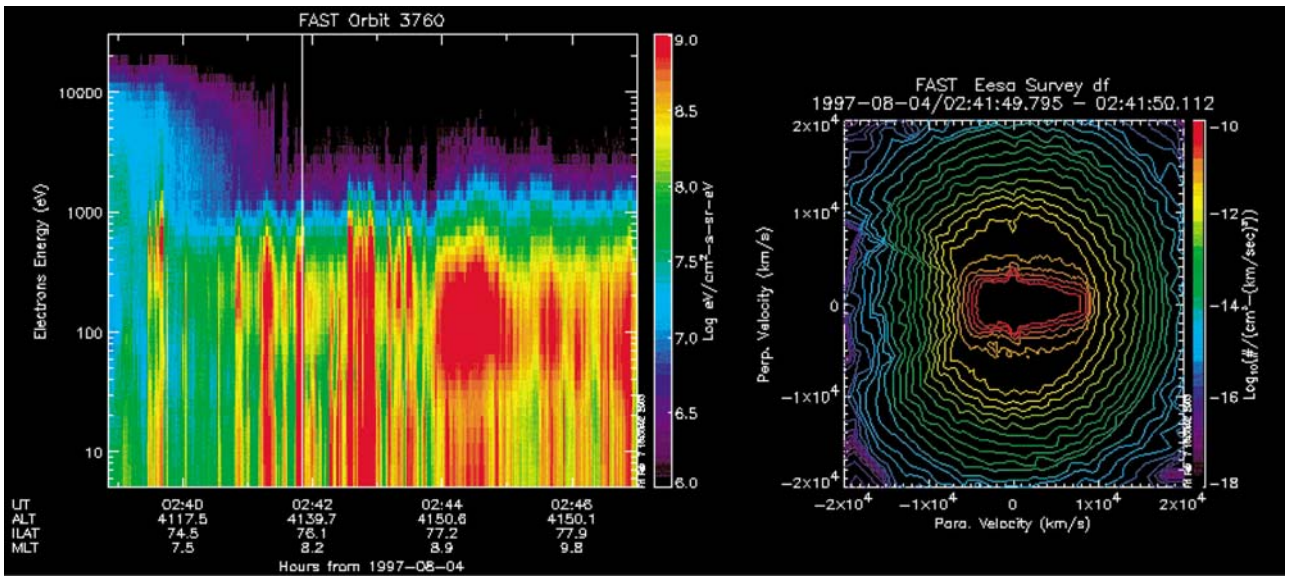

Figure 5. FAST electron observations on 4 August 1997. Left is the electron energy spectrum, which *Zhou et al.* [2003] described. Right is electrons in phase space at the time shown by the vertical line in the spectrum. The phase space density contours have been restricted to values less than 10^{-10} s^3 cm^{-3} km^{-3} so that the pitch angle structure can be seen more clearly. This approach also has the effect of excluding phase space density contours for lower-energy electrons (visible as a hole at the center). The loss cone is clearly visible on left, and the distribution near the center shows that the low-energy electrons move along the field line in both directions. This signature is considered an effect of kinetic Alfvén waves.

al., 2001; *Chaston et al.*, 2005] and velocity shearing [*Seyler*, 1988]. For our shock compression case, the kinetic Alfvén waves were very likely generated by the magnetic reconnection on the dayside magnetopause because of the magnetopause erosion seen in Figures 3 and 4.

[22] As a manifestation of the low-latitude magnetopause erosion, the cusp low-latitude boundary moved equatorward from 28°N at 0809 UT to 11°S at 0818 UT (in Figure 4 for the 4 kR contour), which corresponds to an equatorward moving of 1.6° MLAT at a speed of 18 ± 0.4 km min^{-1} (if contours at ~3.5 and ~4.5 kR are also used for this estimation). As a result, the cusp expanded and reached a meridional width of ~1.6° in latitude at ~1120 MLT, which is increased by a factor of ~2. In previous studies, significant latitudinal motions of the cusp low-latitude boundary (i.e., the open and closed file line boundary) were toward the equator at ~30 km min^{-1} in an IMF B_z southward turning from ~5 to −4 nT [*Sandholt et al.*, 1998c] and at ~20 km min^{-1} with the IMF B_z near zero and B_y between −4 and −6 nT [*Sandholt et al.*, 1998b]. In both cases the solar wind ram pressure was low at 2–3 nPa. In our event, which has an abrupt pressure change from 3 to 6 nPa, the low-latitude boundary moved southward with a speed of ~18 km min^{-1}, which is at about the same speed of the two previous reconnection events. The similar speed indicates that the sudden enhancement in the solar wind ram pressure did not lead to an evident high reconnection rate as expected by the theory of *Song and Lysak* [1994]. Their theory shows that when the solar wind dynamic pressure is large, the magnetopause current sheet becomes thin locally, which allows magnetic reconnection to take place. But the reconnection rate may be affected by the nearby solar wind circumstance. In our case, the downstream solar wind dynamic pressure was higher than normal at 7–9 nPa. However, the solar wind speed was low at ~350 km s^{-1}. The removal of the reconnected magnetic flux could have been retarded because of the slow solar wind, so the reconnection was slowed down. In addition, the IMF B_z was near zero and turned to northward, during which the reconnection rate is lower than that during a southward B_z with a normal solar wind pressure. How solar wind pressure affects dayside reconnection remains a controversial issue [see *Boudouridis et al.*, 2007 and references therein].

4.3. Conclusions

[23] We conclude that shock aurora forms caused by the shock compression are closely related to field line status. The enhanced diffuse aurora is mainly on closed field lines. The northern edge of the diffuse aurora (caused by hard electrons) marks the boundary between open and closed field lines, and the red arcs (caused by soft electrons) are mainly intensified along the boundary and present a different procedure of the particle acceleration. These phenomena again confirm that the diffuse aurora at 557.7 nm serves as a proxy of closed magnetic field lines and that the red arcs are the manifestation of the dayside reconnection.

[24] The bright diffuse aurora is caused by more high-energy electrons falling into the loss cone because of the enhanced pitch angle scattering that result from instabilities or because of an enlarged loss cone that is caused by the enhanced magnetic field intensity at the equator. The aurora expands equatorward and antisunward along the oval when shock moves tailward. This scenario implies that the antisunward propagating shock aurora and the dayside subaurora patches seen from space are mainly diffuse aurora.

[25] In this study the auroral signatures and speculated mechanisms are consistent with those revealed by in situ particle and wave observations studied previously [*Zhou et*

al., 2003]. The implication of the consistence is that shock aurora forms are ionospheric diagnoses of particle acceleration occurring in the magnetosphere or in the magnetopause boundary layer.

[26] **Acknowledgments.** The results reported here represent one aspect of research carried out by the Jet Propulsion Laboratory, California Institute of Technology, under a contract with NASA. Xiaoyan Zhou thanks Adolfo F. Vinas for his helpful discussion about the interplanetary shock. Joran Moen thanks the Norwegian Polar Institute for hosting the University of Oslo's optical instrumentation at Ny-Ålesund, Svalbard, and thanks Espen Trondsen and Bjorn Lybekk at the University of Oslo for processing the optical data used in this paper. Financial support has been provided by the Norwegian Research Council and the Air Force Office of Scientific Research, Air Force Material Command, USAF, under grant FA8655-06-1-3060.

[27] Zuyin Pu thanks the reviewers for their assistance in evaluating this paper.

References

Boudouridis, A., L. R. Lyons, E. Zesta, and J. M. Ruohoniemi (2007), Dayside reconnection enhancement resulting from a solar wind dynamic pressure increase, *J. Geophys. Res.*, *112*, A06201, doi:10.1029/2006JA012141.

Chaston, C. C., et al. (2005), Drift-kinetic Alfvén waves observed near a reconnection X line in the Earth's magnetopause, *Phys. Rev. Lett.*, *95*, 065002, doi:10.1103/PhysRevLett.95.065002.

Chaston, C. C., C. Salem, J. W. Bonnell, C. W. Carlson, R. E. Ergun, R. J. Strangeway, and J. P. McFadden (2008), The turbulent Alfvénic aurora, *Phys. Rev. Lett.*, *100*, 175003, doi:10.1103/PhysRevLett.100.175003.

Eather, R. H. (1985), Polar cusp dynamics, *J. Geophys. Res.*, *90*(A2), 1569–1576, doi:10.1029/JA090iA02p01569.

Farrugia, C. J., P. E. Sandholt, W. F. Denig, and R. B. Torbert (1998), Observation of a correspondence between poleward moving auroral forms and stepped cusp ion precipitation, *J. Geophys. Res.*, *103*(A5), 9309–9315, doi:10.1029/97JA02882.

Fuselier, S. A., S. P. Gary, M. F. Thomsen, E. S. Claflin, B. Hubert, B. R. Sandel, and T. Immel (2004), Generation of transient dayside subauroral proton precipitation, *J. Geophys. Res.*, *109*, A12227, doi:10.1029/2004JA010393.

Gary, S., and I. Cairns (1999), Electron temperature anisotropy instabilities: Whistler, electrostatic and *z* mode, *J. Geophys. Res.*, *104*(A9), 19,835–19,842, doi:10.1029/1999JA900296.

Hellinger, P., O. Travnicek, A. Mangeney, and R. Grappin (2003), Hybrid simulations of the expanding solar wind: Temperatures and drift velocities, *Geophys. Res. Lett.*, *30*(5), 1211, doi:10.1029/2002GL016409.

Hubert, B., J. C. Gerard, S. A. Fuselier, and S. B. Mende (2003), Observation of dayside subauroral proton flashes with the IMAGE-FUV imagers, *Geophys. Res. Lett.*, *30*(3), 1145, doi:10.1029/2002GL016464.

Liou, K., C.-C. Wu, R. P. Lepping, P. T. Newell, and C.-I. Meng (2002), Midday sub-auroral patches (MSPs) associated with interplanetary shocks, *Geophys. Res. Lett.*, *29*(16), 1771, doi:10.1029/2001GL014182.

Lorentzen, D. A., and J. Moen (2000), Auroral proton and electron signatures in the dayside aurora, *J. Geophys. Res.*, *105*(A6), 12,733–12,745, doi:10.1029/1999JA900405.

Lorentzen, D. A., C. S. Deehr, J. I. Minow, R. W. Smith, H. C. Stenbaek-Neielsen, F. Sigernes, R. L. Arnoldy, and K. Lynch (1996), SCIFER-dayside auroral signatures of magnetospheric energetic electrons, *Geophys. Res. Lett.*, *23*(14), 1885–1888, doi:10.1029/96GL00593.

Lysak, R. L., and W. Lotko (1996), On the dispersion relation for shear Alfvén waves, *J. Geophys. Res.*, *101*(A3), 5085–5094, doi:10.1029/95JA03712.

McKenna-Lawlor, S. M. P., et al. (2002), Arrival times of Flare/Halo CME associated shocks at the Earth: Comparison of the predictions of three numerical models with these observations, *Ann. Geophys.*, *20*, 917–935.

Mende, S. B., D. M. Klumpar, S. A. Fuselier, and B. J. Anderson (1998), Dayside auroral dynamics: South Pole-AMPTE/CCE observations, *J. Geophys. Res.*, *103*(A4), 6891–6898, doi:10.1029/97JA03235.

Meurant, M., J.-C. Gérard, B. Hubert, V. Coumans, C. Blockx, N. Østgaard, and S. B. Mende (2003), Dynamics of global scale electron and proton precipitation induced by a solar wind pressure pulse, *Geophys. Res. Lett.*, *30*(20), 2032, doi:10.1029/2003GL018017.

Meurant, M., J.-C. Gérard, C. Blockx, B. Hubert, and V. Coumans (2004), Propagation of electron and proton shock-induced aurora and the role of the interplanetary magnetic field and solar wind, *J. Geophys. Res.*, *109*, A10210, doi:10.1029/2004JA010453.

Moen, J., D. A. Lorentzen, and F. Sigernes (1998), Dayside moving auroral forms and bursty proton auroral events in relation to particle boundaries observed by NOAA 12, *J. Geophys. Res.*, *103*(A7), 14,855–14,863, doi:10.1029/97JA02877.

Parks, G. K. (2003), *Physics of Space Plasmas: An Introduction*, 2nd ed., Westview, Boulder, Colo.

Sandholt, P. E., et al. (1994), Cusp/cleft auroral activity in relation to solar wind dynamic pressure, interplanetary magnetic field B_z and B_y, *J. Geophys. Res.*, *99*(A9), 17,323–17,342, doi:10.1029/94JA00679.

Sandholt, P. E., et al. (1996), Auroral signature of lobe reconnection, *Geophys. Res. Lett.*, *23*(14), 1725–1728, doi:10.1029/96GL01846.

Sandholt, P. E., et al. (1998a), A classification of dayside auroral forms and activities as a function of interplanetary magnetic field orientation, *J. Geophys. Res.*, *103*(A10), 23,325–23,346, doi:10.1029/98JA02156.

Sandholt, P., C. Farrugia, J. Moen, and S. Cowley (1998b), Dayside auroral configurations: Responses to southward and northward rotations of the interplanetary magnetic field, *J. Geophys. Res.*, *103*(A9), 20,279–20,295, doi:10.1029/98JA01541.

Sandholt, P., C. J. Farrugia, M. Øieroset, P. Stauning, and W. F. Denig (1998c), Auroral activity associated with unsteady magnetospheric erosion: Observations on December 18, 1990, *J. Geophys. Res.*, *103*(A2), 2309–2317, doi:10.1029/97JA01317.

Sandholt, P. E., H. C. Carlson, and A. Egeland (2002), *Dayside and Polar Cap Aurora*, *Astrophys. Space Sci. Libr.*, vol. 270, Kluwer Acad., Dordrecht, Netherlands.

Seyler, C. E. (1988), Nonlinear 3-D evolution of bounded kinetic Alfvén waves due to shear flow and collisionless tearing instability, *Geophys. Res. Lett.*, *15*(8), 756–759, doi:10.1029/GL015i008p00756.

Shepherd, G., J. Winningham, F. Bunn, and F. Thirkettle (1980), An empirical determination of the production efficiency for auroral 6300-Å emission by energetic electrons, *J. Geophys. Res.*, *85*(A2), 715–721, doi:10.1029/JA085iA02p00715.

Song, Y., and R. L. Lysak (1994), Alfvénon, driven reconnection and the direct generation of the field-aligned current, *Geophys. Res. Lett.*, *21*(17), 1755–1758, doi:10.1029/94GL01327.

Stasiewicz, K., C. Seyler, F. Mozer, G. Gustafsson, J. Pickett, and B. Popielawska (2001), Magnetic bubbles and kinetic Alfvén waves in the high-latitude magnetopause boundary, *J. Geophys. Res.*, *106*(A12), 29,503–29,514, doi:10.1029/2001JA900055.

Tsurutani, B. T., et al. (2001a), Auroral zone dayside precipitation during magnetic storm initial phases, *J. Atmos. Sol. Terr. Phys.*, *63*, 513–522, doi:10.1016/S1364-6826(00)00161-9.

Tsurutani, B. T., X.-Y. Zhou, V. M. Vasyliunas, G. Haerendel, J. K. Arballo, and G. S. Lakhina (2001b), Interplanetary shocks, magnetopause Boundary layers and dayside auroras: The importance of a very small magnetospheric region, *Surv. Geophys.*, *22*(2), 101–130, doi:10.1023/A:1012952414384.

Vorobjev, V. G., O. I. Yagodkina, D. G. Sibeck, K. Liou, and C.-I. Meng (2001), Polar UVI observations of dayside auroral transient events, *J. Geophys. Res.*, *106*(A12), 28,897–28,911, doi:10.1029/2000JA000396.

Wygant, J. R., et al. (2002), Evidence for kinetic Alfvén waves and parallel electron energization at 4–6 R_E altitudes in the plasma sheet boundary layer, *J. Geophys. Res.*, *107*(A8), 1201, doi:10.1029/2001JA900113.

Yahnina, T. A., H. U. Frey, T. Bösinger, and A. G. Yahnin (2008), Evidence for subauroral proton flashes on the dayside as the result of the ion cyclotron interaction, *J. Geophys. Res.*, *113*, A07209, doi:10.1029/2008JA013099.

Zhang, Y., L. J. Paxton, T. J. Immel, H. U. Frey, and S. B. Mende (2002), Sudden solar wind dynamic pressure enhancements and dayside detached auroras: IMAGE and DMSP observations, *J. Geophys. Res.*, *107*, 8001, doi:10.1029/2002JA009355. [Printed *108*(A4), 2003.]

Zhou, X.-Y., and B. T. Tsurutani (1999), Rapid intensification and propagation of the dayside aurora: Large scale interplanetary pressure pulses (fast shocks), *Geophys. Res. Lett.*, *26*(8), 1097–1100, doi:10.1029/1999GL900173.

Zhou, X.-Y., R. J. Strangeway, P. C. Anderson, D. G. Sibeck, B. T. Tsurutani, G. Haerendel, H. U. Frey, and J. K. Arballo (2003), Shock aurora: FAST and DMSP observations, *J. Geophys. Res.*, *108*(A4), 8019, doi:10.1029/2002JA009701.

Zhou, X.-Y., D. Lummerzheim, G. R. Gladstone, S. D. Gunapala, S. B. Bandara, J. Trihne, and L. Herrell (2008), Magnetospheric application of high-altitude long-duration balloon technology: Daylight auroral observations, *Adv. Space Res.*, *42*, 1676–1682, doi:10.1016/j.asr.2007.02.034.

H. C. Carlson, Air Force Office of Science Research, 875 N. Randolph St., Arlington, VA 22203, USA.

K. Fukui, Air Force Research Laboratory, 29 Randolph Rd., Hanscom AFB, MA 01731, USA.

J. I. Moen, Department of Physics, University of Oslo, Oslo, N-0313, Norway.

R. J. Strangeway, Institute of Geophysics and Planetary Physics, UCLA, 405 Hilgard Ave., Los Angeles, CA 90095, USA.

X.-Y. Zhou, Jet Propulsion Laboratory, 4800 Oak Grove Dr., Pasadena, CA 91109, USA. (xiaoyan.zhou@jpl.nasa.gov)